Regime change and oscillation thresholds in recorder-like instruments

Roman Auvray[a] and Benoît Fabre
LAM, Institut Jean Le Rond d'Alembert, UPMC Univ. Paris 06, UMR CNRS 7190, 11 rue de Lourmel, 75015 Paris, France

Pierre-Yves Lagrée
CNRS, Institut Jean Le Rond d'Alembert, UPMC Univ. Paris 06, UMR CNRS 7190, 4 place Jussieu, 75005 Paris, France

(Received 29 November 2010; revised 29 November 2011; accepted 1 December 2011)

Based on results from the literature, a description of sound generation in a recorder is developed. Linear and non-linear analysis are performed to study the dependence of the frequency on the jet velocity. The linear analysis predicts that the frequency is a function of the jet velocity. The non-linear resolution provides information about limit cycle oscillation and hysteretic regime change thresholds. A comparison of the frequency between linear theory and experiments on a modified recorder shows good agreement except at very low jet velocities. Although the predicted threshold for the onset of the first regime shows an important deviation from experiments, the hysteresis of threshold to higher regimes is accurately estimated. Furthermore, a qualitative analysis of the influence of different parameters in the model on the sound generation and regime changes is presented.
 [DOI: 10.1121/1.3672815]

PACS number(s): 43.75.Qr, 43.75.Ef [JW] Pages: 1574–1585

I. INTRODUCTION

The physics of flute-like instruments has been intensively studied since the pioneer works of Helmholtz[1] and Rayleigh.[2] As a first stage, the study of the passive resonances of the pipe allows a fairly good understanding of the instrument makers' choices. This allows a systematic study of the influence of the bore geometry[3,4] and of the precise holes position and geometry.[5]

Many studies deal with the resonance frequencies, but the sounding frequency of the instrument is also affected by the excitation mechanism, including the blowing conditions. The excitation part has been successively described by several authors. Rayleigh and Helmholtz proposed a description in terms of a force acting on the acoustic field, force that is due to the injection flow on the pipe edge (the labium).[1] Based on a simplified fluid dynamical description, more recent models have started to give substantial results comparable with experiments. These developments, mainly led by Coltman,[6,7] Fletcher[8,9] and Elder,[10] demonstrated that the sounding frequency depends on the blowing pressure. During the same period, works in the fields of hydrodynamics were developed, mostly for edge-tone configurations.[11] These significant improvements in fluid mechanics were applied in sound generation models of edge-tones and recorder-like instrument by Crighton,[12] Howe,[13,14] and Nelson.[15]

The combination of these different elements allowed researchers to develop time-domain simulations.[16] Different models, that are based on an accurate description of the jet behavior, describe the sound generation for different blowing conditions and different window geometries.[17] However, the understanding of the different elements that contribute to the oscillation in flute-like instruments has now grown to a point where it becomes difficult to predict the influence of some specific aspects of the model on the oscillation. This difficulty arises because the system is looped and a global resolution of the equations describing and coupling the different elements is lacking. Therefore, it appears interesting to develop tools that permit understanding of the influence of changes in the model on the sound prediction.

Such a model can be useful in the design and construction of the instruments. Even if global resolution could be expected from direct flow simulations, the use of simplified descriptions is justified by the need to obtain a numerically cheap model that permits a systematic variation in parameters, rather than a unique detailed numerical solution for one particular configuration.

The idea of a lumped description, initially proposed by Powell,[18] was developed later by Mc Intyre,[19] Fletcher,[9] and Verge.[20] As discussed by Fabre and Hirschberg,[21] it became common to study the different elements (pipe acoustics, jet behavior, aeroacoustic sources) separately, even if such a separation is hard to justify. The fact that a lumped model must at least include two time delays and non-linear terms made the model's analysis non trivial. Therefore, most papers present analysis of the behavior of these models either from a linearized or time domain point of view using step by step time integration of the equations. The paper of Fletcher[9] is an important exception since it provides a solution of the non-linear problem for prediction of stable limit cycle oscillation. The linearized model is often used to predict the onset threshold of oscillation for low blowing pressure, and also to roughly estimate oscillating frequency as a function of blowing pressure. However, the linearized model can not predict transients of the oscillating system, and

[a]Author to whom correspondence should be addressed. Electronic mail: auvray@lam.jussieu.fr

 0001-4966/2012/131(2)/1574/12/$30.00

therefore can not predict *a priori* the hysteresis between two regimes of oscillation observed experimentally, an important phenomenon for instrument makers and players.

The present paper aims at comparing the predictions of the linearized and the non-linear models, in terms of oscillating frequency, including regime changes, and amplitude. The sound generation mechanism is first outlined by presenting each part of the lumped model extracted from the literature (Sec. II). The solutions of the linearized and non-linear models are presented in Secs. III and IV. Numerical results are discussed in Sec. VI in comparison with experimental data gathered on a modified recorder (Sec. V).

II. SIMPLIFIED MODEL

The auto-oscillation process results from interaction between an unstable flow, the jet, and an acoustic resonator, the pipe. Driven by the pressure applied upstream from the flue, the fluid in the jet travels towards the pipe edge. As the jet is unstable, perturbations develop from the flue exit to the pipe edge. The interaction between the unsteady jet and the pipe edge results into an unsteady force from the wall on the fluid, which is an aeroacoustic source. The pipe acts as a resonator and accumulates acoustic energy in standing waves near the resonance frequencies. The acoustic waves provide the perturbation of the jet at the flue exit, closing the auto-oscillating feedback loop. Another element must be taken into account: vortex shedding occurs at the labium and dissipates part of the acoustic energy accumulated in the resonator.

As it was done in several previous studies,[7,9] the sound-producing mechanism is divided into five parts. The first part is the passive response of the pipe using a one-dimensional approximation. The second part describes the convection and the amplification of a jet perturbation. The third deals with the generation of a perturbation of the jet by the acoustic field at the flue exit. The fourth addresses the aeroacoustic sound source at the labium, and the fifth addresses the vortex losses at the labium.

A. Passive response of the pipe

The description of the recorder is based on an acoustic model adapted from works of Verge[22] and Chaigne.[23] The geometry of the recorder permits a one-dimensional model. Only the first propagating mode (plane wave) is kept, the higher modes being evanescent. A simplified geometry of the recorder is considered as shown in Fig. 1. The model is made of two bores: a large one representing the pipe where the waves propagate and a small one representing the sound source. Following Helmholtz and Rayleigh, the sound source is seen as a force acting at the entrance of the pipe. This force will be discussed later, but for now it is formally represented as a pressure difference Δp. The pressure difference creates an acoustic flow $Q_{ac} = V_{ac} S_w$, with S_w the window section and V_{ac} the Fourier transform of the acoustic velocity v_{ac}. The acoustic flow depends on both pipe and window impedances, Z_p and Z_w:

$$P^+ = Z_p Q_{ac}, \quad P^- = -Z_w Q_{ac}, \tag{1}$$

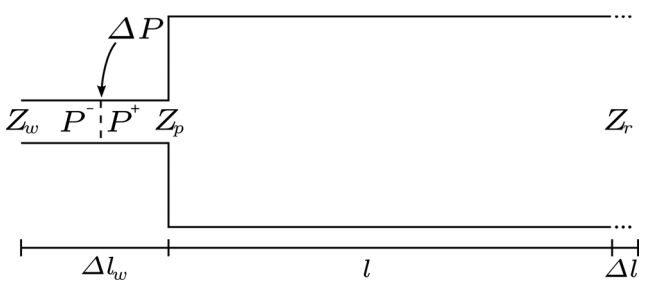

FIG. 1. One-dimensional representation of a recorder. Δl and Δl_w are the end corrections associated with the radiation impedance Z_w and Z_r. Z_p is the pipe impedance seen from the window, and ΔP is the pressure difference representing the force.

where P^+ and P^- are complex pressure amplitudes at the inward and outward sides of the source. The Fourier transform of Δp can be expressed using these complex pressure amplitudes: $\Delta P = P^+ - P^-$. The ratio defined as $Y = V_{ac}/\Delta P$ is the entrance admittance and provides information about how the pipe accumulates acoustic energy for a given source pressure difference. From Eq. (1), one can write

$$Y = S_w^{-1} (Z_p + Z_w)^{-1}. \tag{2}$$

The pipe impedance Z_p is related to the radiation impedance Z_r at the passive end according to the expression

$$Z_p = \frac{\rho c_0}{S} \tanh\left[\Gamma l + \arg\tanh\left(\frac{Z_r}{Z_c}\right)\right], \tag{3}$$

where c_0 is the speed of sound in the air, S the cross section of the pipe, l the length of the pipe and $\Gamma = jk$ (k the wave number) which includes propagating losses.[23–25] The radiation impedance is given by the low frequency approximation:

$$Z_r(\omega) = \frac{\rho c_0}{S}\left(j\frac{\omega}{c}\Delta l + \frac{1}{4}\left(\frac{\omega R}{c}\right)^2\right), \tag{4}$$

where ω is the pulsation, R the radius of the bore and Δl the end correction given by Dalmont.[26] The window impedance Z_w is calculated in the same way by substituting S, R, and Δl in Eq. (4) by S_w the section of the window, R_w the equivalent radius of the window and Δl_w the end correction of the window given by Verge.[16] Moreover, the radiation factor 1/4 in Eq. (4) corresponding to a infinitely thin end is substituted by the infinite flange factor 1/2.[23]

Following Chaigne,[23] using the notation $\eta_i = \arg\tanh(Z_i/Z_c)$ with $i = l, w$, one can write Eq. (2) as

$$Y = Y_c \frac{\cosh(\Gamma l + \eta_l)\cos\eta_w}{\sinh(\Gamma l + \eta_l + \eta_w)}, \tag{5}$$

where $Y_c = S/\rho c_0 S_w$. From this expression, the resonance parameters Y_n, ε_n, and ω_n are numerically extracted and one finally obtains the modal development:

$$Y = \sum_{n=1}^{\infty} \frac{j\omega Y_n}{\omega_n^2 - \omega^2 + j\varepsilon_n \omega_n \omega}, \tag{6}$$

where Y_n, ε_n, and ω_n are the amplitude, the damping coefficient and the pulsation of the nth mode, respectively. Depending on either linear or non-linear analysis, Eq. (5) or Eq. (6) will be used, respectively. Linear study enables numerical estimation of Eq. (5) whereas non-linear approach requires a modal description. The modal decomposition loses information on antiresonance because it is a superposition of poles, not taking zeros into consideration. However, the instrument oscillates near the resonances and solutions are therefore correctly approximated by this decomposition.

The next step is to express the source force as a function of the acoustic variables. The aeroacoustic description of the force requires first a description of the jet oscillations.

B. Amplification and convection of perturbations of the jet

A first approach to study jet dynamics was proposed by Rayleigh[2] and focuses on the linear stability analysis of an infinite shear layer. The flow is split into a mean component and perturbations, the velocity profile $U(y)$ in the downstream direction Ox is a function of the coordinate of the cross-stream direction Oy. The velocity perturbation has the components u and v along Ox and Oy, respectively. The cross stream velocity perturbation defined as an harmonic propagating function $v = \mathbf{v}(y)\exp[i(\omega t - \alpha x)]$ satisfies Rayleigh's equation:

$$[U(y) - c]\left[\frac{d^2\mathbf{v}(y)}{dy^2} - \alpha^2\mathbf{v}(y)\right] - \frac{d^2U(y)}{dy^2}\mathbf{v}(y) = 0, \qquad (7)$$

which involves the wave number α and the phase velocity $c = \omega/\alpha$.

As the pulsation ω is real (spatial analysis), α is complex, its real part corresponding to dispersion and its imaginary part to amplification. The linear analysis consists in finding the eigenvalue α associated with the eigenfunction $\mathbf{v}(y)$ for a given ω. Rayleigh provided analytical solutions for piecewise linear velocity profiles. This eigenvalue problem can be solved numerically for more realistic velocity profile[27] including the traditional Bickley profile. Nolle[28] conducted the resolution for a family of profiles:

$$U(y) = U_0\mathrm{sech}^2(y/b)^k, \qquad (8)$$

which better fit experimental data on organ pipe jets, where U_0 is the centerline velocity and b the half width of the jet ($U(\pm b) = U_0/2$). The integer k enables modification of the Bickley profile ($k = 1$) to a flatter profile. He also computed the solution for low frequency pulsation ω that are relevant to musical acoustics.

The information provided by the linear spatial analysis is that for a given ω, the perturbation is convected on the jet at the phase velocity of perturbation $c_p = \omega/\mathrm{Re}(\alpha)$ with the exponential amplification factor $-\mathrm{Im}(\alpha)$. This description is only valid for small amplitudes of perturbation and for an infinite jet. In recorder-like instruments, the jet emerges from the flue exit of height h, crosses the finite extended window over a distance W and reaches the edge of the labium. For typical value $W/h \sim 4$ found in recorders, it is assumed that the perturbation does not have room to reach amplitudes which induce strong non-linear processes. For high Strouhal number defined as $S_t = Wf/U_B$ with f the frequency and U_B the jet velocity estimated by applying Bernoulli's law from the pressure reservoir to the flue exit, the jet will break down into discrete vortices as described by Holger.[11] The linear description is no longer valid. One can adopt a "discrete vortices" approach arguing that the jet is surrounded by two shear layers. On each of these shear layers, the vorticity concentrates into discrete points due to the shear layer instability.

Moreover, the velocity profile at the flue exit depends on the history of the flow before it emerges in the window. As discussed by Ségoufin,[29] the flue channel has an important effect on the profile. Through Rayleigh's equation [Eq. (7)], the jet velocity profile U modifies the wave number α and even more so the amplification and the phase velocity.

C. Receptivity of the jet

The acoustic field drives the perturbation of the jet flow. This phenomenon is generally called "receptivity." It is considered here that the acoustic field initiates a perturbation of the jet by acting on the vorticity of the shear layers of the jet. While the jet crosses the window, the acoustic field is assumed to be fully defined as a potential flow, and thus the vorticity of the jet is conserved. The effect of the acoustic field can be described as a slight displacement of the flow in the cross stream direction ($v_{ac} \ll U_B$). However, near the sharp edge of the flue exit, the potential flow becomes singular and the vorticity can be generated by flow separation. The initial perturbation of the jet is assumed to be due to the action of the acoustic field at the flue exit, where the flow separation occurs.[21]

Some descriptions of the initial perturbation state that the motion of the jet at $x = 0$ is opposed to the acoustic displacement in such a way that the displacement of the jet remains zero at the flue exit. Even if such a description showed good agreement with experimental data,[20,30] it misses physical grounds since a fluid would oppose a shear rate rather than a displacement. Moreover, this description diverges at low frequency. Attempts have been made to propose a more accurate description of the receptivity based on the work of Nelson.[15] For high Strouhal numbers or thick jets, i.e., when a discrete vortices description seems more appropriate, the initialization of a new vortex at the flue exit is triggered by the change of direction (sign) of the acoustic velocity.[17] There is no simple model for predicting the receptivity. For this reason, the empirical expression for the receptivity proposed by de la Cuadra[31] based on the Schlieren visualization of a jet flowing in a transverse acoustical field is used. The receptivity is assimilated to an equivalent initial transverse displacement of the jet at the separation point. De la Cuadra proposed that the initial transverse displacement of the jet η_0, compared with the height of the flue exit h, depends on the transverse acoustic velocity at the flue exit v_{ac}, compared with the jet velocity:

$$\frac{\eta_0(t)}{h} = \frac{v_{ac}(t)}{U_B}. \qquad (9)$$

The transversal displacement of the jet at a distance x from the flue exit results from the amplification and the convection of the initial perturbation, which is described by

$$\eta(t,x) = e^{\alpha_i x}\eta_0\left(t - x/c_p\right), \tag{10}$$

where α_i and c_p are empirical coefficients, corresponding to the amplification and the phase velocity of a perturbation along the jet, respectively. De la Cuadra[31] proposed a first order approximation of these parameters: $\alpha_i = \beta/h$ and $c_p = \gamma U_B$ where $\beta \sim 0.3$ is the jet spatial amplification and $\gamma \sim 0.4$ is the relative convection velocity. These values are the same order as those found in the literature.[6,32,33]

It is convenient to have a one-dimensional description of the transverse displacement of the jet rather than a full two (three) dimensional flow. It is common[9,20,31] to describe the jet in terms of its centerline and its velocity profile only. In such a description, the initial perturbation is often assimilated to the transverse displacement of the centerline at the flue exit. This is the approach that will be used here. However, even if the separation points of the flow are not affected by the acoustic field, the velocity profile is. Hence, the receptivity phenomenon deserves the development of a more accurate description as suggested by Blanc.[34]

The experimental setup used in order to develop Eqs. (9) and (10) is a simplified copy of a real recorder windway with different flue channel and flue exit geometries. The modification of the flue channel geometry has an effect on the unperturbed velocity profile $U(y)$. As mentioned above it modifies the wave number α and thus α_i and c_p. Secondly, the flue exit shape is known to have important effects on the sound production. Recorder makers pay extreme attention to this matter. According to these observations, the use of a first order approximation for $\alpha_i = \beta/h$ and $c_p = \gamma U_B$ represents a drastic simplification. However, for the sake of having a very basic model, the effects of the flue exit geometry are ignored and a unidimensional description of the jet is used. The jet spatial amplification β and the relative convection velocity γ are critical parameters in the model whose influences on the oscillation of the system should be systematically investigated.

The linear behavior of the perturbation, Eq. (10), is obviously no longer valid when the jet breaks into discrete vortices. For short window opening W such as in the recorder, the approximation presented in Eq. (10) is justified. However, the model will certainly show some unrealistic behaviors at high Strouhal number as found in organ pipes at low blowing pressure.

The transverse displacement of the jet at the labium η is obtained by combining Eqs. (9) and (10):

$$\eta(t) = \frac{he^{\alpha_i W}}{U_B} v_{ac}(t-\tau), \tag{11}$$

where $\tau = W/c_p$ is the convection delay. The reduced jet velocity $\theta = U_B/Wf_1$, where f_1 is the first resonance frequency of the pipe, will be used as control parameter.

D. Jet-labium interaction: Non-linear characteristic

The question of the type of sources involved in the sound production of flute-like instrument started with the so-called Helmholtz/Rayleigh controversy.[21] They finally agreed that since the acoustic pressure is small and the acoustic velocity is large at the window of the instrument, the resonator should be driven by a force source term.

Coltman[6,7] initiated the jet drive model, which is commonly accepted in the literature. In the model, the jet labium interaction is described in terms of air flow. At the labium, the jet is split in two complementary flows. The flow Q_{in} entering in the pipe is separated into an average and an oscillating flow: $Q_{in} = \langle Q_{in} \rangle + Q_1$, where $\langle \cdot \rangle$ indicates averaging over one period. The outward flow is identically described and its oscillating part Q_2 is complementary to Q_1. Both flows Q_1 and Q_2 are injected at positions close to the edge of the labium within the small bore of length Δl_w corresponding to the acoustic length of the window in the one-dimensional model (see Fig. 1). As the acoustic length of the window is small compared with the wavelength, the air between the two injection points is assumed to be incompressible. Applying third Newton's law on this incompressible air mass, and using a formal representation of the force in terms of a pressure difference $\Delta p S_w$ lead to the expression of the pressure difference representing the force which drives the resonator:[20]

$$\Delta p = -\frac{\rho \delta_d}{S_w}\frac{dQ_1}{dt}, \tag{12}$$

where ρ is the air density, $S_w = W H_w$ the window section, H_w the window width, and δ_d the effective acoustical "distance" between the two sources. The exact position of the sources, which determines this distance, is a sensitive parameter of the model. Assuming that each source is at a distance h behind the labium, Verge[22,35] calculated $\delta_d = 4/\pi\sqrt{2hW}$ with the help of conformal mapping of the two dimensional acoustic field.

The flow Q_{in} is related to the jet lateral displacement $\eta(t)$ by the following expression:[22]

$$Q_{in}(t) = H_m \int_{-\infty}^{y_{off}-\eta(t)} U(y)dy, \tag{13}$$

where y_{off} is the offset between the channel exit and the edge, as presented in Fig. 2.

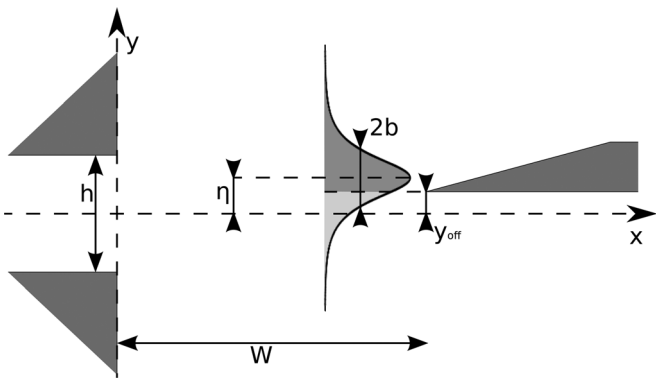

FIG. 2. Window geometry of a recorder. A jet emerges from a flue of height h, and it looks like a Bickley profile jet from far away. It impinges the labium at distance W from the flue exit.

The velocity profile $U(y)$ indirectly affects the amplification of the perturbation, as previously mentioned. It also has a direct effect on the system as it determines the non-linear characteristic of the source through Eq. (13). As shown by Ségoufin[29] and Van Zon,[36] when the length of a straight channel is larger than a critical length, the flow reaches a fully developed Poiseuille velocity profile. The channel of the recorder is actually slightly convergent, so the velocity profile at the end of the channel is expected to be better approximated by a Nolle profile, Eq. (8). However, a Poiseuille flow at the flue exit is assumed. At a distance far enough from the flue exit (few h), because the air is dragged along the jet by viscous entrainment, there is a gradual smoothing of the jet profile. Thus, at the labium the velocity profile is expected to be well approximated by a Bickley profile [$k=1$ in Eq. (8)]. Following Ségoufin, the centerline velocity U_0 is assimilated to the jet velocity U_B estimated by applying Bernoulli's law between the pressure reservoir and the flue exit. Under these assumptions, the half width of the Bickley profile is given by $b=2h/5$ if a Poiseuille flow at the flue exit is assumed.

Using Eqs. (12), (13), and (8) (with $k=1$), finally yields to the pressure-displacement characteristic:

$$\Delta p_{src}(t) = \frac{\rho \delta_d b U_B}{W} \frac{d}{dt}\left[\tanh \frac{\eta(t) - y_{off}}{b}\right]. \tag{14}$$

E. Vortex shedding at the labium

The window of the recorder represents a constriction for the acoustic flow. For large acoustic velocities, the flow separation occurs at the labium resulting in the formation of vortices. The flow separation seen as a free jet[37] dissipates energy that is not recovered by the acoustic field. This mechanism, already mentioned by Coltman[6] and sometimes forgotten in models, is decisive for the determination of the amplitude of the steady oscillation.[38] The flow separation and the subsequent vortices induce a variation of the window pressure[23]

$$\Delta p_{los}(t) = -\frac{1}{2}\rho\left(\frac{v_{ac}(t)}{\alpha_{vc}}\right)^2 \mathrm{sgn}(v_{ac}(t)), \tag{15}$$

in addition to the driven pressure Δp_{src}. The vena contracta factor $\alpha_{vc} \sim 0.6$ is here again a sensitive parameter of the model. The total pressure driving the resonator in the one-dimensional model is then

$$\Delta p(t) = \Delta p_{src}(t) + \Delta p_{los}(t). \tag{16}$$

III. RESOLUTION OF THE LINEARIZED MODEL

The whole system described previously can be represented by a circuit with a feedback loop where Eq. (11) rules a block of amplification and delay, Eqs. (14) and (15) represent non-linear characteristics and Eq. (5) represents a transfer function.

Inspired by the Barkhausen stability criterion used in electronics[39] and by the method used by Powell,[18] it is possible to find a necessary but not sufficient criterion for the establishment of oscillations in the instrument. Indeed, the study of the loop gain G of the linearized equations in the frequency domain leads to two conditions on the existence of oscillation. These two conditions are related to the amplitude and the phase of the linearized loop gain.

If there is no linear contribution of the flow separation Eq. (15), injecting Eqs. (11) and (12) linearized around y_{off} in Eq. (16) leads to the Fourier transform ΔP of Δp:

$$\Delta P(\omega) = \frac{\rho \delta_d U_B}{W} i\omega H(\omega), \tag{17}$$

where

$$H(\omega) = \frac{h e^{\alpha_i W}}{U_B} V_{ac}(\omega) e^{-i\omega\tau} \tag{18}$$

is the Fourier transform of $\eta(t)$. The loop gain defined as $G = Y\Delta P/V_{ac}$ is written:

$$G = \mu Y(\omega) e^{-i\omega\tau} i\omega, \tag{19}$$

where $\mu = h e^{\alpha_i W}\ \rho\delta_d/W$. The first condition for the existence of oscillations is that the phase shift around the loop must be equal to an integer multiple of 2π. This implies that the system oscillates at frequencies given by

$$-\omega_n \tau + \frac{\pi}{2} + \arg(Y(\omega_n)) = 2n\pi, \tag{20}$$

where the integer n represents the hydrodynamic modes of the jet. The first hydrodynamic mode corresponds to $n=0$, higher modes by increasing values of n. For instance, aeolian sounds obtained at lower jet velocities correspond to the second, or higher, jet mode $n \geq 1$.

For a given n, Eq. (20) has several solutions. For each of these solutions ω_s, the oscillation can start if the modulus of the gain evaluated at ω_s is higher than unity. Figure 3 is obtained by numerically solving Eq. (20) with $n=0$, and injecting this solution in the modulus of the gain G.

Solutions result from a balance between the jet and the resonator phase shifts, $\omega\tau$ and $\arg(Y(\omega))$, respectively. For each value of the reduced jet velocity θ, the frequency is entirely determined by the phase condition. Thus, the shape of the solution in the (θ, f) plane is directly linked with the phase response of the resonator (Fig. 3).

Solutions at which the oscillation can naturally grow are plotted with a solid line on Fig. 3. These solutions correspond to frequencies where the gain is large enough. The resonator sufficiently amplifies the oscillation for frequencies close to the pipe resonances.

Oscillation can not start below a particular jet velocity θ_0, namely the onset threshold of oscillation. Furthermore, there exists a range of velocities $I_h = [\theta_{2\to1}, \theta_{1\to2}]$ in which oscillations can start on both first and second pipe regimes (acoustic modes). Considering the history of the oscillation, for a jet velocity θ in the range I_h, it is possible to have either a first regime or a second regime sound. Since above $\theta_{1\to2}$ the oscillation can only occur on the second regime, $\theta_{1\to2}$ represents a threshold of regime change from the first regime to the second one. Reversely, $\theta_{2\to1}$ corresponds to the threshold of regime change

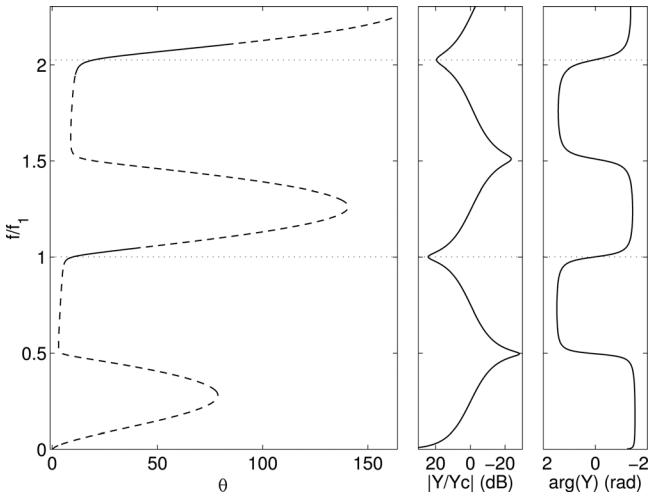

FIG. 3. (Left) Dimensionless frequency obtained by analysis of the linearized model versus reduced jet velocity $\theta = U_B/Wf_1$ for the first and second regimes. The solid line corresponds to frequency whose associated gain is higher than unity. (Right) Amplitude and phase associated with the dimensionless admittance Y/Y_c. The dashed line represents the resonance frequencies. Note that the reduced jet velocity increases over a factor of 150 in order to show the full range of solutions, but for musical purposes, it never exceeds about 30. Moreover, both assumptions of the linear analysis and the model are no longer valid for high jet velocities.

from the second regime to the first one. The existence of the common range I_h makes an hysteresis possible. At this stage, the end of a regime of oscillation seems to be determined by the jet velocity at which the loop gain falls under unity.

The linearized model predicts an exponential growth of oscillation. Obviously, a stable limit cycle can not be predicted without including non-linear terms, see Eqs. (14) and (15). These non-linear terms can significantly change the behavior of the oscillator. A more detailed numerical study of the system is thus needed to estimate the hysteresis thresholds.

IV. RESOLUTION OF THE COMPLETE NON-LINEAR MODEL

A. Quasi-steady dimensionless equations

First establish the system which rules the dynamics of the oscillator. Using Eqs. (11), (14), (15), (16) and the inverse Fourier transform of Eq. (6) leads to

$$\begin{aligned} &v_{ac}(t) = \sum_n v_n(t), \\ &v_n'' + \varepsilon_n \omega_n v_n' + \omega_n^2 v_n \\ &= Y_n \frac{d}{dt}\left\{ \frac{\rho \delta_d b U_B}{W} \frac{d}{dt}\left[\tanh\left(\frac{h e^{\alpha_i W}}{U_B b} \right.\right.\right. \\ &\left.\left.\left. \times v_{ac}(t-\tau) - \frac{y_{off}}{b} \right)\right] - \frac{\rho}{2\alpha_{vc}^2} v_{ac}^2(t) \mathrm{sgn}(v_{ac}(t)) \right\}, \end{aligned} \tag{21}$$

where $'$ and $''$ denote first and second differentiations with respect to time and where the acoustic velocity is written using a modal decomposition consistent with Eq. (6). Note that Eq. (21) is based on the assumption of a constant jet velocity U_B. This equation remains exact for a time-dependant jet velocity. In order to solve these equations numerically, it is convenient to make them dimensionless. A dimensionless time is defined as $\tilde{t} = \omega_1 t$ where ω_1 is the pulsation of the first mode in Eq. (6), and a dimensionless jet transverse displacement is defined as

$$y(\tilde{t}) = \frac{\eta((\tilde{t}+\tilde{\tau})/\omega_1)}{b} = \frac{h e^{\alpha_i W}}{U_B b} v_{ac}(\tilde{t}/\omega_1). \tag{22}$$

As it was done with the acoustic velocity v_{ac}, the dimensionless displacement is written using a modal decomposition: $y = \Sigma_n y_n$. Note that this variable change introduces the time-dependant jet velocity U_B increasing the complexity of the system. To deal with a problem as simple as possible, numerical calculations are performed under quasi-steady assumptions. To do so, the jet velocity U_B as a function of the dimensionless time $\tilde{t}$ must follow the conditions:

$$\begin{aligned} &U_B(\tilde{t}) \simeq U_B(\tilde{t}+\tilde{\tau}), \\ &U_B(\tilde{t}) \simeq U_B(\tilde{t}+2\pi). \\ &\frac{dU_B(\tilde{t})}{d\tilde{t}} \ll U_B(\tilde{t}). \end{aligned} \tag{23}$$

The two first conditions state that the jet velocity must not vary over one period and over the delay $\tilde{\tau}$. The last condition states that the variation of the jet velocity is negligible with respect to the jet velocity value. By using a Taylor expansion of $U_B(\tilde{t}+\tilde{\tau}) \simeq U_B(\tilde{t}) + \tilde{\tau} dU_B/d\tilde{t} + O(\tilde{\tau})$, the combination of the three conditions leads to the global condition:

$$\max_{c_p}(\tilde{\tau}, 2\pi) \frac{dU_B}{d\tilde{t}} \ll U_B, \tag{24}$$

since $\tilde{\tau}$ only varies because of $c_p = \gamma U_B$.

Injecting Eq. (22) and the new time $\tilde{t}$ in Eq. (21) finally leads to the dimensionless system:

$$\begin{aligned} &y(\tilde{t}) = \sum_n y_n(\tilde{t}), \\ &\ddot{y}_n + \varepsilon_n \nu_n \dot{y}_n + \nu_n^2 y_n \\ &= \mu_n \frac{d^2}{d\tilde{t}^2} \tanh(y(\tilde{t}-\tilde{\tau}) - y_0) - \zeta_n \frac{d}{d\tilde{t}} |y|^2, \end{aligned} \tag{25}$$

where $\mu_n = \mu Y_n$, $\zeta_n = \rho b U_B Y_n / 2\, h {\alpha_{vc}}^2 \omega_1 e^{\alpha_i W}$, $y_0 = y_{off}/b$, $\nu_n = \omega_n/\omega_1$, and where $\dot{}$ and $\ddot{}$ denote the first and second differentiations with respect to $\tilde{t}$.

The system (25) is a set of damped harmonic oscillator coupled by non-linear functions. Further, each equation is a neutral delay differential equation (DDE), where the dynamics depend on a delay $\tilde{\tau}$ that appears in a derivative term of the variable y_n. A quick look at Eq. (25) shows that oscillation can start only if the damping term $\varepsilon_n \nu_n$ is lower than the source term μ_n (the non-linear damping being negligible at low amplitudes of oscillations). The previous section investigated this behavior by performing an analysis of the linearized model. A complete solution can be numerically calculated.

B. Numerical calculation

Delay differential equations occur in many domains such as population dynamics or control engineering. Many solvers have been developed but time-varying delay is usually not allowed in most of them. For the purpose of this study, a solver has been developed allowing quasi-steady variations of parameters such as the jet velocity U_B, and thus the delay $\tilde{\tau}$. It is an iterative algorithm based on a fourth order Runge Kutta method. For each step p, the delayed sample $y(p\Delta t - \tilde{\tau})$ is estimated by linear interpolation of the two previous samples $y([p - \|\tilde{\tau}/\Delta t - 1\|]\Delta t)$ and $y([p - \|\tilde{\tau}/\Delta t + 1\|]\Delta t)$, where Δt is the time-step and where $\|\cdot\|$ denotes the nearest integer function. The differentiation of the delay τ is neglected as a consequence of condition (23).

The resolution is run over a time T_s with three modes for different values of the model parameters: the amount of non-linear losses with α_{vc}, the jet spatial amplification β, and the relative jet velocity γ. For each triplet (α_{vc}, β, γ), the jet velocity slowly varies in time from U_{min} to U_{max} with a triangle shape. Thus $|dU_B/d\tilde{t}| = (U_{max} - U_{min})/2T_s$, and the global quasi-steady condition (23) is rewritten:

$$T_s \gg \frac{\omega_1 W(U_{max} - U_{min})}{2\gamma_{min} U_{min}^2}, \tag{26}$$

where $\gamma_{min} = 0.2$ is the smallest γ over all the runs. The oscillation is initiated by holding $y(\tilde{t} < 0)$ constant at an arbitrary value. It results in a short transient at the beginning of the run after which the system evolves freely.

The fundamental frequency of the output and the associated amplitude are estimated by taking the maximum of a short time Fourier transform with a Hanning window. The values of parameters used in computation are summarized in Table I. The dimensionless acoustic velocity v_{ac}/U_B extracted from y by using Eq. (22) depends on the ratio of sections S/S_w since $Y_c = S/\rho c_0 S_w$ in Eq. (5). The numerical calculation and a classical method used by Fletcher[9] (slowly varying parameter) are compared in the Appendix.

C. Sensitivity of the model

The solver permits to independently vary parameters of the model. The investigation of the sensitivity of the model focuses on three parameters. The first one is the importance of the non-linear effects associated with the flow separation at the labium, which is studied by adjusting the vena contracta coefficient α_{vc}. Secondly, the loop gain is studied by adjusting the jet spatial amplification β. Finally, the delay τ is studied by adjusting the relative convection velocity γ. Each of these parameters are sensitive points of the model since they are experimentally obtained and/or represent elements varying according to the different authors. Moreover, they include other sensitive parameters. For instance the jet spatial amplification β allows the modification of the loop gain as the distance between the two sources δ_d could. Lastly, each of these parameters can also be linked to a geometrical or a tunable element of instrument making.

Figure 4 presents the oscillating frequencies obtained by linear analysis for three values of the relative convection velocity $\gamma = 0.2$, 0.4, or 0.6. The delay τ is modified by varying the relative convection velocity, thus the phase condition (20) is modified. As a result, the available frequencies are shifted and the associated oscillation thresholds are changed. Figure 4 also presents the oscillating frequencies of the solution of the complete non-linear model for a relative convection velocity $\gamma = 0.4$. An overview of the solution provided by the solver highlights general trends of the model. Firstly, the way the frequency depends on jet velocity is slightly modified, compared with the linear analysis, by the introduction of non-linear processes. Secondly, the thresholds of regime change are strongly affected by the non-linear processes. Thirdly, the model predicts numerous aeolian regimes for low jet velocity. As mentioned previously, at high Strouhal (low jet velocity), the model overestimates these regimes. Dequand[17] showed that when a "discrete vortex" description is more appropriate (high Strouhal number or low value of W/h) the jet drive model overestimates sound production. As a consequence, the onset threshold of oscillation θ_0 depends on the presence of these aeolian regimes. The first regime stops when the oscillator behaves on the second or on the third aeolian regimes while decreasing jet velocity. Because of this shortcomings, the investigation of the influences of the parameters is restricted at the transition between the first and the second regime.

TABLE I. Geometrical parameters of the recorder used in the experiment, modal parameters of the resonator and computation parameters.

Recorder parameters	$W = 4$ mm	$H = 12$ mm	$\phi_{in} = 19$ mm
	$h = 0.8$ mm	$l = 265$ mm	$y_{off} = 0$ mm
Modal parameters	$\omega_1 = 3547$ rad/s	$\varepsilon_1 = 3.966\text{e-}2$	$Y_1 = 28.45$ kg/m^2
	$\nu_2 = \omega_2/\omega_1 = 2.023$	$\varepsilon_2 = 3.184\text{e-}2$	$Y_2 = 24.88$ kg/m^2
	$\nu_3 = \omega_3/\omega_1 = 3.066$	$\varepsilon_3 = 2.847\text{e-}2$	$Y_3 = 20.24$ kg/m^2
Computation parameters	$T_s = 3\ 10^5$	$\beta = 0.2 \rightarrow 0.6$	$\gamma = 0.2 \rightarrow 0.6$
	$\rho = 1.19$ kg/m^3	$\alpha_{vc} = 0.5 \rightarrow 0.9$	$U_B = 6 \rightleftarrows 75$ m/s

The influence of the relative convection velocity γ is well described in the framework of the linearized model analysis: adding non-linear source and losses does not modify the convection effects. Figure 5 shows the evolution of the regime change thresholds $\theta_{1\rightarrow 2}$ and $\theta_{2\rightarrow 1}$ as functions of the jet spatial amplification β and for different magnitude of non-linear losses (α_{vc}). An increase of the loop gain enlarges the available range of frequency for both regimes: the two thresholds move away from each other. The evolution of the threshold $\theta_{1\rightarrow 2}$ with respect to the jet spatial amplification β is not monotonous. This suggests that, at least for the transition from the first to the second regime, the threshold is determined by a competition between the two non-linear processes (source and damping).

The non-linear losses due to vortex shedding at the labium are crucial for the prediction of the amplitude of oscillation, but they also affect the transition from the first to the second regime. Reversely, the non-linear losses mechanism does not affect the threshold $\theta_{2\rightarrow 1}$. The two non-linear processes are not strongly involved in the beginning of the second regime because the predictions of the complete and the linearized model are only barely shifted. These observations call for an

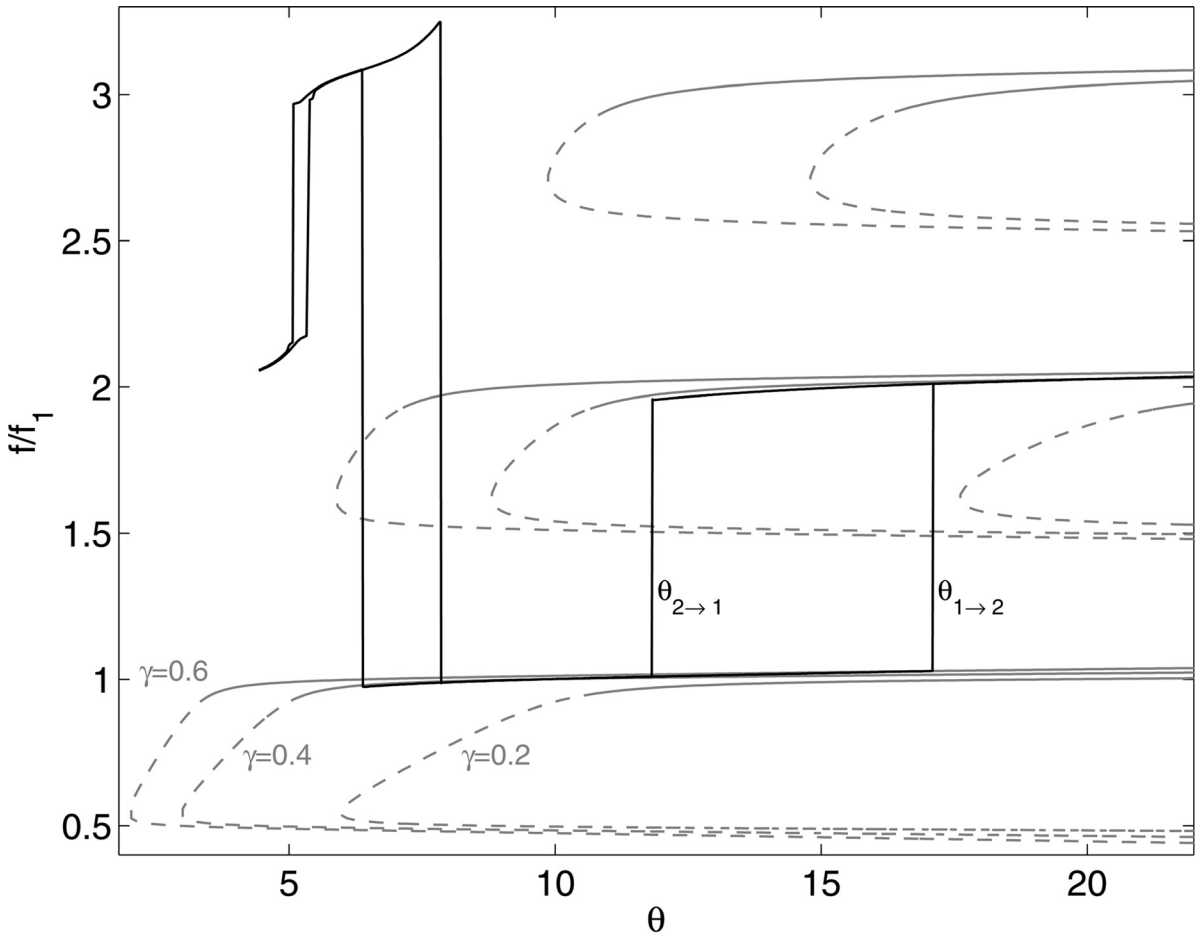

FIG. 4. (Gray lines) Dimensionless frequency obtained by analysis of the linearized model versus reduced jet velocity $\theta = U_B/Wf_1$ for three values of the relative convection velocity $\gamma = 0.2$, 0.4, 0.6. The solid lines correspond to frequency whose associated gain is higher than 1. (Black lines) Dimensionless frequency predicted by the complete model and obtained by numerical calculation versus $\theta = U_B/Wf_1$ for $\beta = 0.3$, $\gamma = 0.4$ and $\alpha_{vc} = 0.6$.

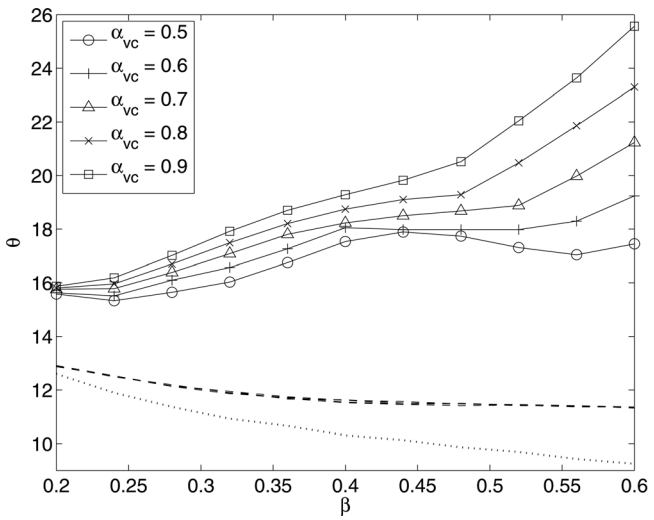

FIG. 5. Regime change thresholds $\theta_{1\to2}$ (solid line) and $\theta_{2\to1}$ (dashed line) estimated by numerical calculation of the complete model versus jet spatial amplification β for different values of the vena contracta coefficient α_{vc} associated to the flow separation at the labium. Note that the thresholds $\theta_{2\to1}$ overlay for the five values of α_{vc}. The threshold $\theta_{2\to1}$ predicted by the analysis of the linearized model is also plotted in dotted line (at the bottom).

estimation of the influence of both source and damping terms with respect to the reduced jet velocity. But first, the predictions of the model have to be compared with measurements made on the experimental setup presented in the next section.

V. EXPERIMENTAL SETUP

A modified Zen-On Bressan recorder is used keeping the mouthpiece (sound production piece) and replacing the resonator by a cylindrical pipe whose inner diameter $\phi = 19$ mm matches the inner diameter of the mouthpiece of the recorder. The brass cylindrical pipe has a wall thickness 0.5 mm and the resulting length of the recorder from the flue exit to the passive end is $l = 265$ mm. The window of size $W = 4$ mm and $H_m = 12$ mm is surrounded by "ears" of length $l_{ears} = 7.3$ mm. The labium presents a sharp angle of $\approx$15 degrees and is slightly curved in the transverse direction. The flue windway has a length of 46 mm and is slightly convergent between the input (13.6×1.5 mm^2) to the output (12.5×0.98 mm^2). The cross section of the flue channel is a segment of annulus. The other geometrical parameters are listed in Table I. The use of a cylindrical pipe makes the calculation of the passive response of the pipe easier. The use of an optimized recorder mouthpiece facilitates the sound production. The ratio $W/h \sim 4$ is convenient compared with

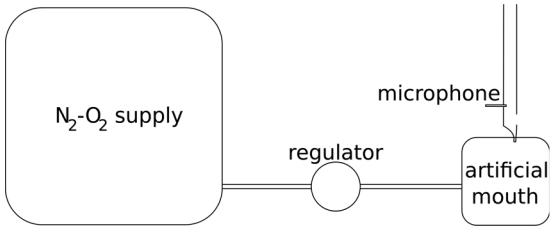

FIG. 6. Experimental setup. Compressed N_2-O_2 mixture is sent to the artificial mouth to sound the recorder. The blowing pressure is adjusted using the regulator. The artificial mouth pressure is measured using a pressure sensor. Acoustic oscillation is measured at a close distance from the window.

the restriction of the model. This recorder model was already studied by Lyons,[4] at least for the passive response of the instrument. Compressed N_2-O_2 mixture in the same proportion as air is sent into an artificial mouth in which the flute is plugged as shown on Fig. 6. The artificial mouth is a cylindrical cavity of volume 1.5 dm^3 filled with an absorbent material in order to damp the cavity resonances. The pressure in the mouth p_m is measured by means of an Endevco 8507 C dynamic pressure sensor. The acoustic pressure is measured in the bore of the recorder with a microphone B&K 4938 at 16 mm from the cork. The microphone is mounted flush in the wall of the recorder mouthpiece at an angle of $\pi/2$ with respect to the axis of the window.

The cavity pressure is adjusted manually with a pressure regulator. The measurement procedure consists in slowly increasing the blowing pressure p_m until the instrument overblows on the second regime of oscillation, and then slowly decreasing the pressure p_m back to zero. The whole measurement lasts about 3 min, which ensures a quasi-steady variation of the cavity pressure. The jet velocity is estimated by applying Bernoulli's law: $U_B = \sqrt{2p_m/\rho}$. The fundamental frequency f_0 is extracted from the acoustic pressure by using the algorithm YIN[40] and the associated amplitude p_{ac} is estimated by taking the maximum of a short time Fourier transform near the frequency predicted by YIN. The amplitude p of the pressure mode is then given by

$$p = \frac{p_{ac}}{\left|\sin\left(\frac{2\pi f_0}{c} x_m\right)\right|}, \tag{27}$$

where x_m is the distance between the microphone and the passive end, including the radiation end correction $\Delta l = 0.3 \times 19$ mm. The amplitude of the pressure mode is converted into a dimensionless acoustic velocity by using $pS/S_w \rho c U_B$ (including the ratio of pipe and window cross sections S/S_w). Results are shown in Figs. 7 and 8.

As other authors have already found (for instance Meissner[41] on a Helmholtz resonator), the fundamental frequency has a different dependence on the jet velocity in two

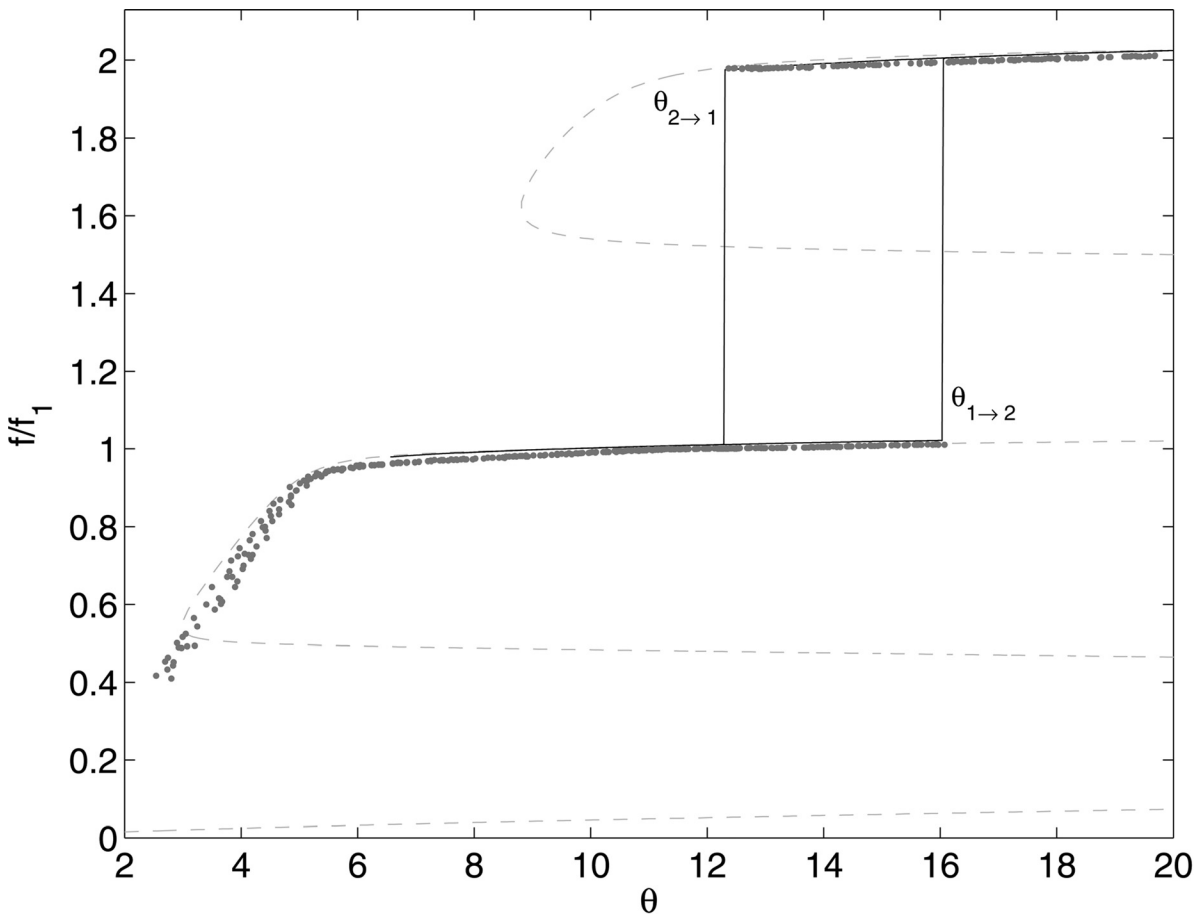

FIG. 7. Dimensionless frequency f/f_1 versus reduced jet velocity $\theta = U_B/Wf_1$ for experiment (dot) and numerical resolution of the complete model (solid line) for $\alpha_{vc} = 0.7$, $\beta = 0.26$, $\gamma = 0.4$. The aeolian regimes predicted by the model are not plotted. For information, frequency predicted by the linearized model is plotted in dashed gray line.

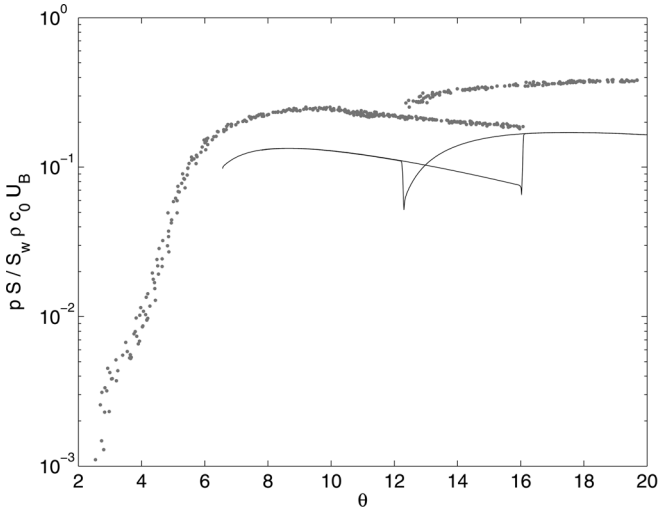

FIG. 8. Dimensionless amplitude $p/\rho c_0 U_B$ versus reduced jet velocity $\theta = U_B W f_1$ for experiment (dot) and numerical resolution of the complete model (solid line) for $\alpha_{vc} = 0.7$, $\beta = 0.26$, $\gamma = 0.4$.

different ranges. At low jet velocity, the frequency rapidly increases with the jet velocity θ. For higher jet velocities, the frequency slowly increases until it reaches the regime change and the system overblows. On the second regime, one can observe the same trend: f_0 slowly increases with the velocity. The amplitude of oscillation is plotted on Fig. 8. Amplitude measurements of the two first regimes are consistent with the literature.[30] The first regime amplitude rapidly grows for low jet velocity and slowly decreases for higher jet velocities. The dimensionless amplitude of the second regime is close to that of the first (Fig. 8), as already noticed by Verge,[30] Dequand,[17] and Fabre.[38]

VI. DISCUSSION

As discussed in Sec. IV C, three main parameters of the model are adjustable (the relative convection velocity γ, the jet spatial amplification β and the vena contracta coefficient α_{vc}). Figure 7 presents the oscillating frequency measured in this experimental setup compared to that predicted by the model for particular values of the model parameters. The agreement is fairly good for the prediction of the frequency for the first and second oscillating regimes, except at low jet velocities. The hysteresis thresholds are accurately predicted for values of α_{vc}, β, and γ close to those found in the literature.[6,31–33] However, the model underestimates the amplitude of oscillation by a factor of 2 (Fig. 8). Because of the complex balance between the source and the dissipation terms, the relation between the adjustable parameters and the amplitude of the limit cycle is not straightforward. For instance, the numerical value of the jet spatial amplification ($\beta = 0.26$) is slightly lower than those found in the literature ($\beta \approx 0.5$) and is expected to have a great influence on the amplitude of oscillation. The linear losses (viscous, thermal, and radiation) are difficult to estimate accurately and also affect the source/dissipation balance. The set of values of the parameters has been adjusted to match the frequency and the hysteresis.

The shift of frequency associated with control blowing pressure (or jet mean velocity) is an important characteristic of an instrument as seen from the player's and maker's point of view. However, the hysteretic jump of frequency between different oscillating regimes is even more crucial to the musical applications. The model presented in the previous sections permits one to test the influence of several parameters on the oscillation thresholds.

Because the model overestimates aeolian regimes at low blowing conditions (high Strouhal number), the discussion is restricted to the first and second regimes of oscillation. The thresholds between the first and the second regimes for increasing ($\theta_{1\to2}$) and decreasing ($\theta_{2\to1}$) jet velocities are presented on Fig. 5, for different values of the non-linear losses (α_{vc}), as a function of the linear loop gain (β). The lower limit of oscillation on the second regime predicted by the linearized model is also plotted for comparison. The first striking point is that the transition from the second regime to the first one ($\theta_{2\to1}$) is independent from the amplitude of the non-linear losses (α_{vc}) while the transition from the first regime to the second one ($\theta_{1\to2}$) is strongly affected by the non-linear losses. Furthermore, the transition $\theta_{2\to1}$ predicted by the analysis of the linearized model is close to the one observed by the complete non-linear model. In contrast, the transition $\theta_{1\to2}$ predicted by the linearized model (not plotted on Fig. 5) is at least one order of magnitude higher than the one predicted by the complete non-linear model. As a result, the threshold $\theta_{1\to2}$ for increasing jet velocity appears to be controlled by the non-linear losses while the threshold $\theta_{2\to1}$ for decreasing jet velocity is independent of linear losses.

There are two types of non-linearities in the model. The first one is induced by the saturation of the jet drive mechanism when the amplitude of the jet oscillation becomes wider than the half jet width [Eq. (14)]. The second is associated with the flow separation at the labium [Eq. (15)]. The relative contributions of these two terms have already been studied by Fabre.[38] The solver presented here permits one to quantify these contributions. For the purpose of comparison, the acoustic power $\mathcal{P}_{JD}$ generated by the jet drive source term, the acoustic power $\mathcal{P}_{Li}$ associated with the linear dissipation by radiation and propagation of the mode i, and the acoustic power $\mathcal{P}_{VX}$ dissipated by the flow separation at the labium are calculated as

$$\begin{aligned} \mathcal{P}_{JD} &= \langle S_w v_{ac} \Delta p_{src} \rangle, \\ \mathcal{P}_{Li} &= \langle -S_w \varepsilon_i \omega_i Y_i^{-1} v_i v_{ac} \rangle, \\ \mathcal{P}_{VX} &= \langle S_w v_{ac} \Delta p_{los} \rangle, \end{aligned} \tag{28}$$

where $\langle \cdot \rangle$ indicates averaging over a period. The three contributions are plotted on Fig. 9 as function of the reduced jet velocity for oscillation on the first and second regimes. The energy balance $\mathcal{P}_{JD} = \mathcal{P}_{VX} + \Sigma_i \mathcal{P}_{Li}$ is verified. As discussed by Fabre,[38] the decrease of the sound production $\mathcal{P}_{JD}$ after its maximum value, observed here on both first and second regimes, is due to the evolution of the phase shift between the source term and the acoustic velocity. As expected from the behavior of the model observed on Fig. 5, the power

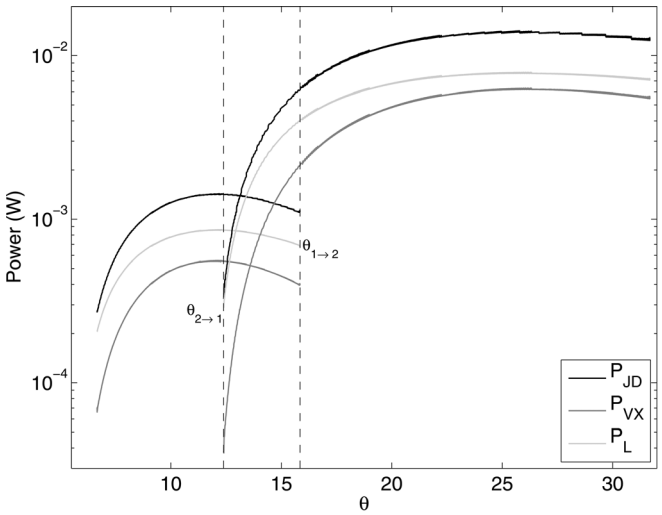

FIG. 9. Powers associated with the source ($\mathcal{P}_{JD}$), with the losses due to the flow separation at the labium ($\mathcal{P}_{VX}$) and with the losses due to propagation and dispersion ($\mathcal{P}_L$) versus reduced jet velocity $\theta = U_B/Wf_1$ for the two first regimes and for $\alpha_{vc} = 0.7$, $\beta = 0.26$, $\gamma = 0.4$. Dashed lines represents the two thresholds $\theta_{1\to2}$ and $\theta_{2\to1}$. The powers are estimated by numerical calculation. For each regime, the energy brought by the source at low jet velocity is balanced by the linear losses whereas at higher jet velocity both losses mechanisms have to be taken into account.

$\mathcal{P}_{VX}$ associated with the flow separation at the labium represents a small contribution to the energy balance of the system for the lowest jet velocities of both first and second regimes. This contribution becomes larger as the jet velocity increases, approaching the contribution of linear losses for the second regime.

VII. CONCLUSION

This paper presented a model designed from different elements of the literature that showed good agreement with the experimental data presented here. Notably it predicted the frequency dependency on the blowing pressure and the thresholds of regime change. Crude approximations were made in order to ease numerical solution, and are determining factors of the restrictions of the model. Both models of jet and sources are inappropriate at high Strouhal number corresponding to very low blowing pressures. The passive description relies on low frequency assumptions. However, it provides fair results for higher blowing pressures.

The effects of each part of the model have been identified. The amplitude of the limit cycle depends on the jet velocity: different mechanisms rule the dynamics at different jet velocities. The onset of oscillation is well described by a linearization of the source model. For higher jet velocity, the saturation of the jet drive mechanism, followed by the saturation of the vortex shedding mechanism, are determinant in the prediction of amplitudes of oscillation. The end of the first regime depends on the strongest non-linear process, namely the flow separation at the labium. By contrast, the onset of the second regime is determined by the variation of the loop gain and of the relative convection velocity.

This model could provide elements of understanding relevant to an instrument maker's choices. For instance, the loop gain has a link with the quality factor of the resonator and modifies both the onset of oscillation and the frequency shift with blowing pressure. The vena contracta coefficient of the flow separation seems to control the regime change threshold and depends on the presence of sharp edges in the resonator. The model also provides a consistent framework to study spectral enhancement. Further improvements should focus on the jet and source descriptions covering a wider range of control blowing pressure and geometrical conditions.

ACKNOWLEDGMENTS

The authors would like to thank Laurent Quartier for his help in preparing the experimental setup, Indiana Wollman for her helpful suggestions about the manuscript, Raymonds Michael Winters for correcting the English and the two anonymous reviewers for their productive and relevant comments and suggestions.

APPENDIX: METHOD OF SLOWLY VARYING PARAMETERS

To solve the set of equations (25), it is possible to use the method of slowly varying parameters. As the resonator is described by several modes, solutions of (25) are expected to be of the form

$$y_n(\tilde{t}) = A_n(\tilde{t})\sin(\nu_n\tilde{t} + \theta_n(\tilde{t})), \tag{A1}$$

where the amplitude A_n and the phase θ_n are slowly varying functions of the time $\tilde{t}$. Their variations over a period are neglected. By applying slowly varying calculation,[42] equations on amplitude A_n and phase θ_n are written:

$$\begin{aligned}
\nu_n\dot{A}_n &= -\frac{\nu_n\varepsilon_n}{2}A_n \\
&\quad - \frac{\mu_n}{2\pi}\int_0^{2\pi}\frac{d^2}{dt_n^2}[\tanh(y(t-\tau))]\cos t_n dt_n \\
&\quad + \frac{\zeta_n}{2\pi}\int_0^{2\pi}\frac{d}{dt_n}|y(t)|^2\cos t_n dt_n, \\
\nu_n A_n\dot{\theta}_n &= -A_n\frac{\mu_n}{2\pi}\int_0^{2\pi}\frac{d^2}{dt^2}[\tanh(y(t-\tau))]\sin t_n dt_n \\
&\quad + \frac{\zeta_n}{2\pi}\int_0^{2\pi}\frac{d}{dt_n}|y(t)|^2\sin t_n dt_n,
\end{aligned} \tag{A2}$$

where $t_n = \nu_n t + \theta_n$. The main difficulty of the method of slowly varying parameters consists in the evaluation of the projections against sinusoidal functions. The last term of the right-hand side of Eq. (A2) could be developed in terms of series since $y = \Sigma_n y_n$.

As explained by Fletcher,[9] the expansion of non-linear terms leads to a new series where the nth oscillating term is given by $\cos((\nu_i \pm \nu_j \pm \nu_k \pm \cdots)t)$ where $i \pm j \pm k \pm \cdots = \pm n$. The method consists of keeping the terms which correspond to the pulsation of the mode (considering $\nu_n \simeq n\nu_1$) and neglecting the others. The other non-linear term (tanh) requires a Taylor expansion in order to perform the same calculation. Thus, the whole resolution of this problem involves

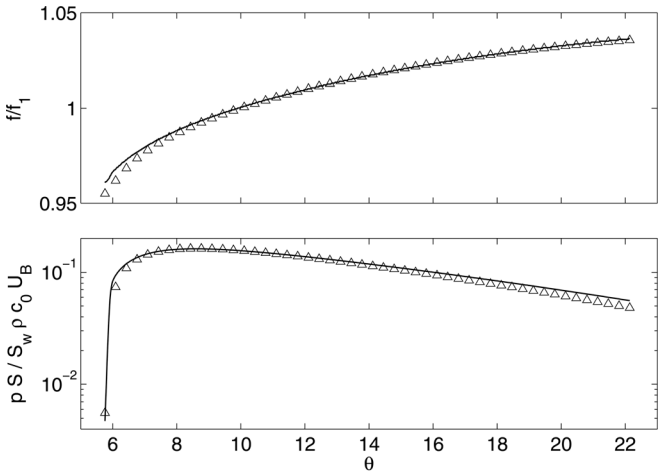

FIG. 10. Dimensionless frequency f/f_1 and dimensionless amplitude $pS/S_w\rho c_0 U_B$ versus reduced jet velocity $\theta = U_B/Wf_1$ for the method of slowly varying parameters (triangle) and for the numerical calculation described in Sec. IV (solid line) for $\alpha_{vc} = 0.6$, $\beta = 0.3$, $\gamma = 0.4$, $U_{min} = 13$ m/s, $U_{max} = 50$ m/s, and $T_s = 150\,000$.

a lot of algebra. The calculation is limited to one mode. For each step of integration of Eq. (A2) the projections against sinusoidal functions are numerically estimated avoiding the expansion of the non-linear function.

Figure 10 compares the amplitude and the frequency estimated by the solver described in Sec. IV with those predicted by the method of slowly varying parameters for different values of the reduced jet velocity θ. Both methods of resolution predict the same trend as that described in Sec. V. However, the predictions are slightly shifted, especially when the amplitude of oscillation is smaller than its maximum value.

[1]H. von Helmholtz, *On the Sensation of Tones* (Dover, New York, 1954), Chap. 6.
[2]J. W. S. Rayleigh, *The Theory of Sound* (Dover, New York, 1945), Vol. 2, Chap. 21.
[3]J. W. Coltman, "Resonance and sounding frequencies of the flute," J. Acoust. Soc. Am. **40**, 99–107 (1966).
[4]D. H. Lyons, "Resonance frequencies of the recorder (english flute)," J. Acoust. Soc. Am. **70**, 1239–1247 (1981).
[5]A. H. Benade, "On the mathematical theory of woodwind finger holes," J. Acoust. Soc. Am. **32**, 1591–1608 (1960).
[6]J. W. Coltman, "Sounding mechanism of the flute and organ pipe," J. Acoust. Soc. Am. **44**, 983–992 (1968).
[7]J. W. Coltman, "Jet drive mechanisms in edge tones and organ pipes," J. Acoust. Soc. Am. **60**, 725–733 (1976).
[8]N. H. Fletcher, "Jet drive mechanism in organ pipes," J. Acoust. Soc. Am. **60**, 481–483 (1976).
[9]N. H. Fletcher, "Sound production by organ flue pipes," J. Acoust. Soc. Am. **60**, 926–936 (1976).
[10]S. Elder, "On the mechanism of sound production in organ pipes," J. Acoust. Soc. Am. **54**, 1554–1564 (1973).
[11]D. K. Holger, T. A. Wilson, and G. S. Beavers, "Fluid mechanics of the edgetone," J. Acoust. Soc. Am. **62**, 1116–1128 (1977).
[12]D. Crighton, "The edgetone feedback cycle. linear theory for the operating stages," J. Fluid Mech. **234**, 361–391 (1992).
[13]M. S. Howe, "Contributions to the theory of aerodynamic sound, with application to excess jet noise and the theory of the flute," J. Fluid Mech. **71**, 625–673 (1975).
[14]M. S. Howe, "The role of displacement thickness fluctuations in hydroacoustics, and the jet drive mechanism of the flue organ pipe," Proc. R. Soc. London A **374**, 543–568 (1981).
[15]P. A. Nelson, N. A. Halbiwell, and P. E. Doak, "Fluid dynamics of flow excited resonance part 2," J. Sound Vib. **91**, 375–402 (1983).
[16]M.-P. Verge and A. Hirschberg, "Time-domain simulation of aeroacoustic sources in flute-like instruments," J. Acoust. Soc. Am. **100**, 2811–2812 (1996).
[17]S. Dequand, J. F. H. Willems, M. Leroux, R. Vullings, M. van Weert, C. Thieulot, and A. Hirschberg, "Simplified models of flue instruments: Influence of mouth geometry on the sound source," J. Acoust. Soc. Am. **113**, 1724–1735 (2003).
[18]A. Powell, "On the edgetone," J. Acoust. Soc. Am. **33**, 395–409 (1961).
[19]M. E. McIntyre, R. T. Schumacher, and J. Woodhouse, "On the oscillations of musical instruments," J. Acoust. Soc. Am. **74**, 1325–1343 (1983).
[20]M.-P. Verge, A. Hirschberg, and R. Caussé, "Sound production in recorderlike instruments. II. A simulation model," J. Acoust. Soc. Am. **101**, 2925–2939 (1997).
[21]B. Fabre and A. Hirschberg, "Physical modeling of flue instruments: A review of lumped models," Acust. Acta Acust. **86**, 599–610 (2000).
[22]M.-P. Verge, B. Fabre, W. E. A. Mahu, A. Hirschberg, R. R. van Hassel, A. P. J. Wijnands, J. J. de Vries, and C. J. Hogendoorn, "Jet formation and jet velocity fluctuations in a flue organ pipe," J. Acoust. Soc. Am. **95**, 1119–1132 (1994).
[23]A. Chaigne and J. Kergomard, *Acoustique des Instruments de Musique* (*Acoustics of Musical Instruments*) (Belin, Paris, 2008), Chaps. 5, 7, 10.
[24]D. H. Keefe, "Acoustical wave propagation in cylindrical ducts: Transmission line parameter approximations for isothermal and nonisothermal boundary conditions," J. Acoust. Soc. Am. **75**, 58–62 (1984).
[25]A. D. Pierce, *Acoustics: An Introduction to Its Physical Principles and Applications* (McGraw-Hill, New York, 1981), Chap. 10.
[26]J.-P. Dalmont, C. Nederveen, and N. Joly, "Radiation impedance of tubes with different flanges: Numerical and experimental investigations," J. Sound Vib. **244**, 505–534 (2001).
[27]G. E. Mattingly and W. O. Criminale, "Disturbance characteristics in a plane jet," Phys. Fluids **14**, 2258–2264 (1971).
[28]A. W. Nolle, "Sinuous instability of a planar air jet: propagation parameters and acoustic excitation," J. Acoust. Soc. Am. **103**, 3690–3705 (1998).
[29]C. Ségoufin, B. Fabre, M. P. Verge, A. Hirschberg, and A. P. J. Wijnands, "Experimental study of the influence of the mouth geometry on sound production in a recorder-like instrument: Windway length and chamfers," Acust. Acta Acust. **86**, 649–661(13) (2000).
[30]M.-P. Verge, B. Fabre, A. Hirschberg, and A. P. J. Wijnands, "Sound production in recorderlike instruments. I. Dimensionless amplitude of the internal acoustic field," J. Acoust. Soc. Am. **101**, 2914–2924 (1997).
[31]P. de la Cuadra, "The sound of oscillating air jets: Physics, modeling and simulation in flute-like instruments," Ph.D. thesis, University of Stanford, 2005.
[32]S. Thwaites and N. H. Fletcher, "Acoustic admittance of organ pipe jets," J. Acoust. Soc. Am. **74**, 400–408 (1983).
[33]S. Yoshikawa, "Jet-wave amplification in organ pipes," J. Acoust. Soc. Am. **103**, 2706–2717 (1998).
[34]F. Blanc, P.-Y. Lagrée, P. De La Cuadra, and B. Fabre, "Influence of the geometrical parameters in flue instruments on the vorticity modulation near the separation points of the jet," in *Proceedings of Acoustics'08*, ASA-EAA, Paris, France (2008).
[35]M.-P. Verge, R. Causse, B. Fabre, A. Hirschberg, A. P. J. Wijnands, and A. van Steenbergen, "Jet oscillations and jet drive in recorder-like instruments," Acust. Acta Acust. **2**, 403–419 (1994).
[36]J. van Zon, A. Hirschberg, and J. Gilbert, "Flow through the reed channel of a single reed music instrument," Colloq. Phys. Suppl. **2**, 821–824 (1990).
[37]U. Ingard and H. Ising, "Acoustic nonlinearity of an orifice," J. Acoust. Soc. Am. **42**, 6–17 (1967).
[38]B. Fabre, A. Hirschberg, and A. P. J. Wijnands, "Vortex shedding in steady oscillation of a flue organ pipe," Acust. Acta Acust. **82**, 863–877 (1996).
[39]T. F. Bogart, *Electronics Devices and Circuits* (MacMillan, New York, 1993), Chap. 12.
[40]A. de Cheveigné and H. Kawahara, "Yin, a fundamental frequency estimator for speech and music," J. Acout. Soc. Am. **111**, 1917–1930 (2002).
[41]M. Meissner, "Aerodynamically excited acoustic oscillations in cavity resonator exposed to an air jet," Acust. Acta Acust. **88**, 170–180 (2002).
[42]A. H. Nayfeh, *Perturbation Methods* (John Wiley, New York, 2000), Chap. 5.